

# Investigation on the sawing temperature in ultrasonic vibration assisted diamond wire sawing monocrystalline silicon

Yan Wang<sup>\*</sup>, Li-Xing Song, Jian-Guo Liu, Rui Wang, Bo-Cheng Zhao

School of Mechanical Engineering, University of Shanghai for Science and Technology, Shanghai 200093, China



## ARTICLE INFO

**Keywords:**  
Monocrystalline silicon  
Diamond wire saw  
Ultrasonic vibration  
Sawing temperature

## ABSTRACT

In this paper, the effects of different sawing parameters (wire saw speed  $v_s$ , feed rate  $v_w$ , workpiece rotation speed  $n_w$ ) and ultrasonic vibration on the sawing temperature in diamond wire sawing monocrystalline silicon were studied. Firstly, the finite element model in diamond wire sawing monocrystalline silicon is established with respect to the thermal transient analysis in ANSYS. Then the influence of different sawing parameters and ultrasonic vibration on the sawing temperature during the sawing process is simulated and analyzed. Finally, the experiment of diamond wire sawing monocrystalline silicon is accomplished to validate the simulation results. The results show that the highest sawing temperature in conventional diamond wire sawing (CWS) is 27.9 °C and that in ultrasonic vibration assisted diamond wire sawing (UAWS) is 29.9 °C. In addition, with the increase of wire saw speed, feed rate and workpiece rotation speed, the sawing temperature increases averagely by about 3.6 °C, 1.6 °C, and 2.0 °C respectively in CWS, and the sawing temperature in UAWS increases averagely by 3.7 °C, 1.5 °C and 1.5 °C. The sawing temperature in UAWS is about 1.5 °C higher than that in CWS under the same sawing parameters. The average error between the simulation and experimental results of highest sawing temperature is 8.6% and the maximum error is 14%, which verifies the simulation model.

## 1. Introduction

As one of the important hard and brittle semiconductor materials, monocrystalline silicon is widely used in aerospace, semiconductor manufacturing, microelectronics industry, precision optics and other high-tech fields [1,2]. It is hard to machine hard and brittle crystal materials because of its high strength, high wear resistance and high hardness and brittleness. Wire saw sawing technology is a method suitable for machining hard and brittle materials and it has the advantages of narrow sawing kerf, small sawing force, good surface quality and small thickness of slice, etc. Moreover, the wire sawing technology is gradually becoming an important process technology for sawing the hard and brittle semiconductor materials [3,4]. The slurry wire sawing was mainly used for wafer production in 1990s, while processing, the workpiece is fed against the wire saw without any other form of motion and sawed into wafers. In order to improve the sawing efficiency and reduce the cost and pollution, the fixed diamond wire saw was invented in recent years and it has replaced the slurry wire saw that was widely used before as the main sawing technology [5,6]. However, because of some difficult-to-cut materials such as high hardness and brittleness

materials, it is difficult for conventional diamond wire sawing (CWS) achieving high sawing efficiency and better workpiece quality, the ultrasonic vibration assisted diamond wire sawing (UAWS) was proposed, which added transverse ultrasonic vibration to the diamond wire saw cutting the workpiece. And it is found in a lot of experiment research that the ultrasonic vibration can obviously improve the machining efficiency and the wafer surface quality [7,8].

Temperature is one of important physical parameters during machining process. During sawing process, as the workpiece is cut continuously by the diamond wire saw, almost all the energy consumed is converted into heat, of which about 1/3 to 1/2 is absorbed by the workpiece. Temperature variation in the sawing area of workpiece during sawing will leads to uneven distribution of residual stress in the wafer, which causes undesirable warp [9]. The sawing process is one of the key processes in chip manufacturing and it is the initial step of the entire process. Therefore, the machining quality and the deformation of the slice play an important role in the whole subsequent machining process. It is vital to study the sawing temperature during the diamond wire sawing monocrystalline silicon [10]. The experiment of fixed diamond wire sawing sapphire was carried out on the JXQ-1201 single-wire

\* Corresponding author.

E-mail address: [yanwang909909@163.com](mailto:yanwang909909@163.com) (Y. Wang).

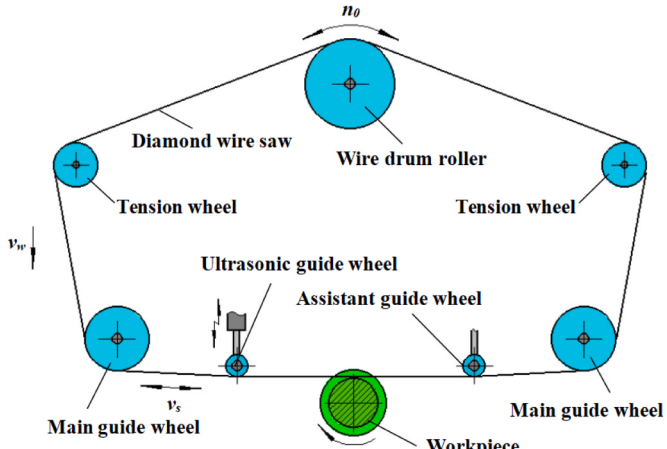


Fig. 1. Schematic of UAWS monocrystalline silicon.

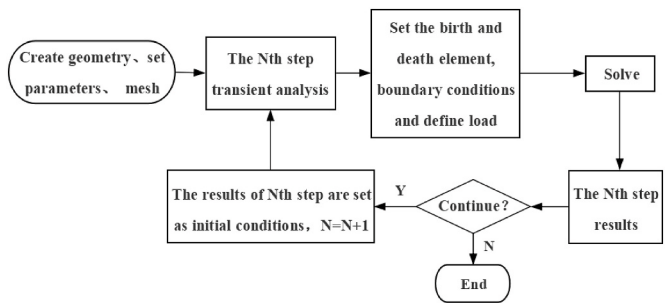


Fig. 2. Schematic of finite element analysis flow.

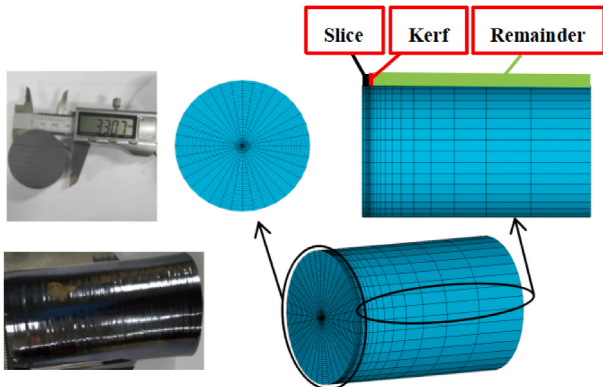


Fig. 3. Finite element model of monocrystalline silicon.

**Table 1**  
Material parameters of monocrystalline silicon.

Parameters	Value
Elasticity modulus (Pa)	1.9e11
Poisson ratio	0.064–0.28
Density (kg/m <sup>3</sup> )	2330
Heat capacity (J/(kg·K))	700
Conductivity (W/(m·K))	146
Coefficient of thermal expansion (1/K)	2.62e-6

sawing machine tool by Huang Xuerun [11] et al. The ImageIR 5325 infrared thermal imager and the Tropel flatness meter were used to detect the sawing temperature and the wafer deformation, which

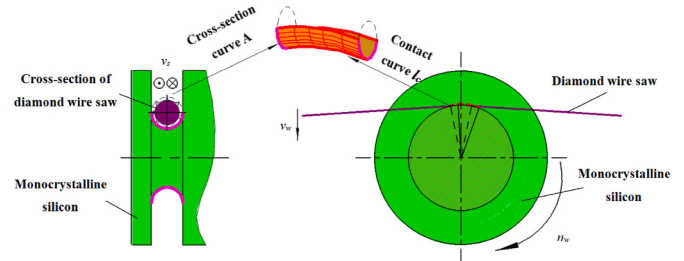


Fig. 4. Schematic of the contact area S.

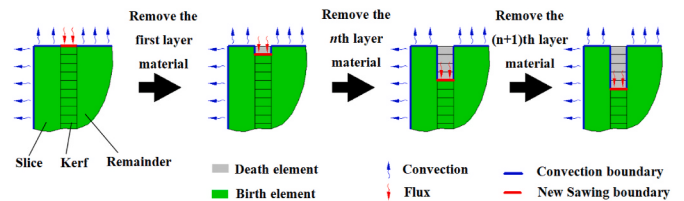


Fig. 5. The birth-death element and loading process.

verified the temperature field distribution model of wafer established by ANSYS software. A theoretical model of temperature field in multi-wire cutting silicon was set up by Wang Jiancheng [12] et al. The distribution of temperature field was analyzed and the effects of processing parameters on the temperature field was studied. The temperature of the cutting area in multi-wire cutting silicon was studied by Jiang Yu [13] et al. And the temperature field during wire sawing was simulated and analyzed by ANSYS based on the application of finite element method in heat transfer. The temperature distribution in fixed diamond wire saw cutting silicon and that in slurry wire saw cutting were simulated by Xu Zonghua [14]. The FLUENT software was used to analyze the temperature change in different kinds of wire sawing and the experiment of wire sawing silicon was conducted. It showed that the trends of temperature curves in the simulation and the experiment are roughly the same. The slice shape features of wire sawing sapphire and silicon carbide were obtained by Li Xixi through experiment research and the slice warp was measured by the Tropel flatness gauge [15]. The temperature change in multi-wire saw cutting silicon was simulated by Sumeet Bhagava [9] et al. It is found that the temperature increases first then reduces as the cutting position changes from the wafer center to the edge. The infrared temperature sensor was used by Yoshinori Abe [16] et al. to measure the temperature during multi-wire sawing silicon. The results showed that the temperature of silicon ingot rises a maximum of roughly 13 °C. The temperature distribution in the sawing area of multi-wire sawing sapphire ingot was measured by Shinya Moriyama [17] et al. using the thermal infrared imager, and the dynamic temperature of the ingot was also measured by type K thermocouples. The temperature change during multi-wire sawing silicon ingot and the wafer warp were simulated and analyzed by Toshiro Yamada [18] et al. An experiment of temperature measurement was accomplished using thermocouples, which verified the finite element model.

Most research results above are focused on the temperature during slurry wire sawing and the workpiece is fed against the wire saw without any other form of motion and sawed into wafers during processing. Many experimental researches show that compared with slurry wire saw, the fixed diamond wire saw has the advantages of narrower kerf, higher sawing efficiency and smaller surface roughness value of workpiece. The sawing force is smaller and the surface quality of the workpiece is better when the workpiece is rotated than those when the workpiece is not rotated during processing. Moreover, ultrasonic vibration assistance can improve the sawing efficiency and reduce the sawing force in fixed diamond wire sawing. However, there are few studies on temperature in UAWS hard and brittle material which is

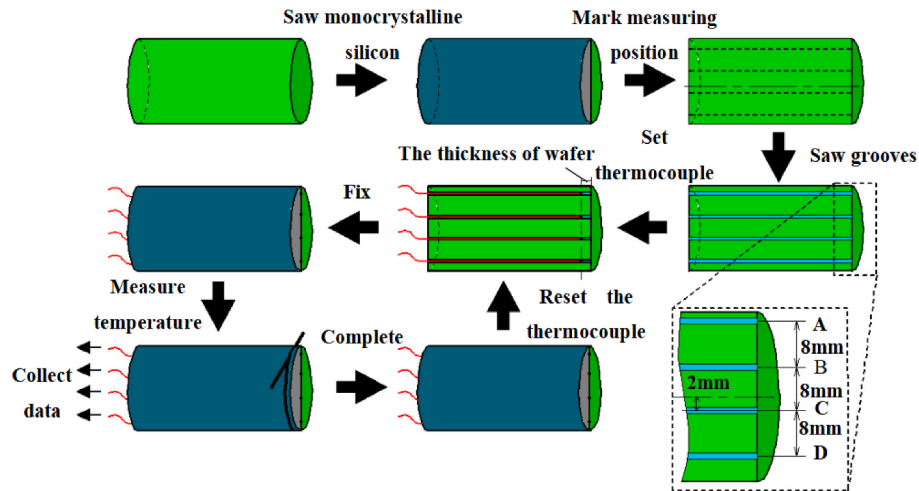


Fig. 6. Flow chart of thermocouples setup.

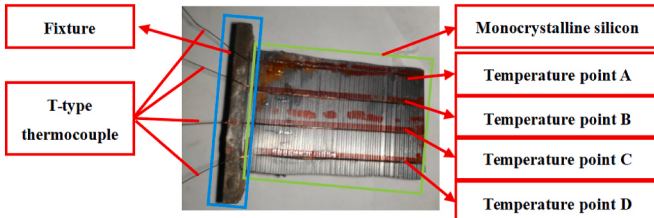


Fig. 7. Image of temperature measuring points.

rotated during sawing process. In this paper, the finite element model of temperature in UAWS monocrystalline silicon is established. The temperature in different positions during UAWS and the temperature field on the wafer surface are obtained. In addition, the experiment of measuring sawing temperature during UAWS monocrystalline silicon by thermocouples is accomplished. The temperature curves at different positions with time are obtained and the effects of sawing parameters and ultrasonic vibration on the sawing temperature are analyzed.

## 2. The finite element model of sawing temperature

### 2.1. Principle of UAWS monocrystalline silicon

**Fig. 1** is the schematic of UAWS monocrystalline silicon. The diamond wire saw is intertwined with a wire drum roller, tension wheels, main guide wheels, ultrasonic guide wheel and assistant guide wheel forming a closed loop. During sawing process, the diamond wire saw is moved at a wire saw speed  $v_s$  driven by the wire drum roller. In addition, the workpiece is rotated at speed  $n_w$  and the integral structure such as the wrapping droller and guide wheels are moved together downwards at same feed rate  $v_w$ . The diamond wire saw is stretched by the tension wheels with constant tension forces from a pair of air cylinders. The ultrasonic vibration is applied on the wire saw by a self-designed assistant device that is installed on the diamond wire saw machine tool. When the ultrasonic vibration device is turned on, the wire saw is vibrated under the ultrasonic excitation and saw the workpiece.

### 2.2. The flow of finite element simulation analysis on temperature

The flow of finite element simulation analysis on temperature in diamond wire sawing monocrystalline silicon is shown in **Fig. 2**. Firstly, the 3D thermal analysis model of monocrystalline silicon was established according to the actual size of workpiece. Then, the transient analysis and calculation of temperature field are carried out by setting

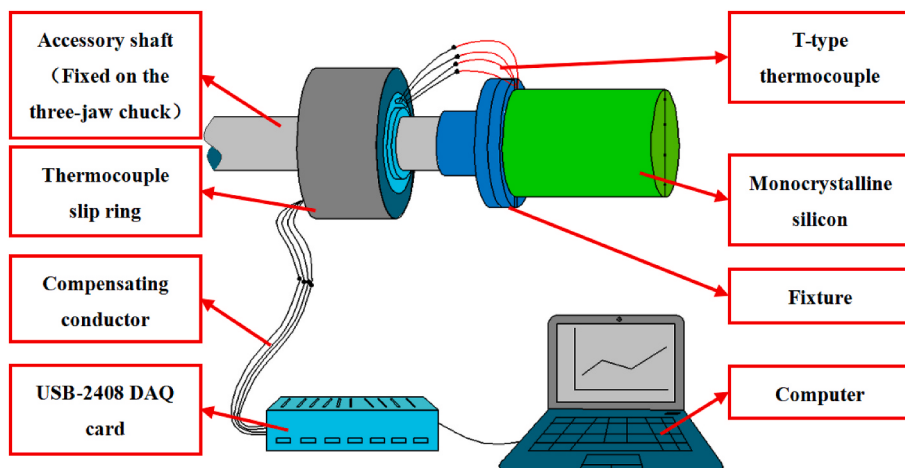


Fig. 8. Schematic of temperature measuring.

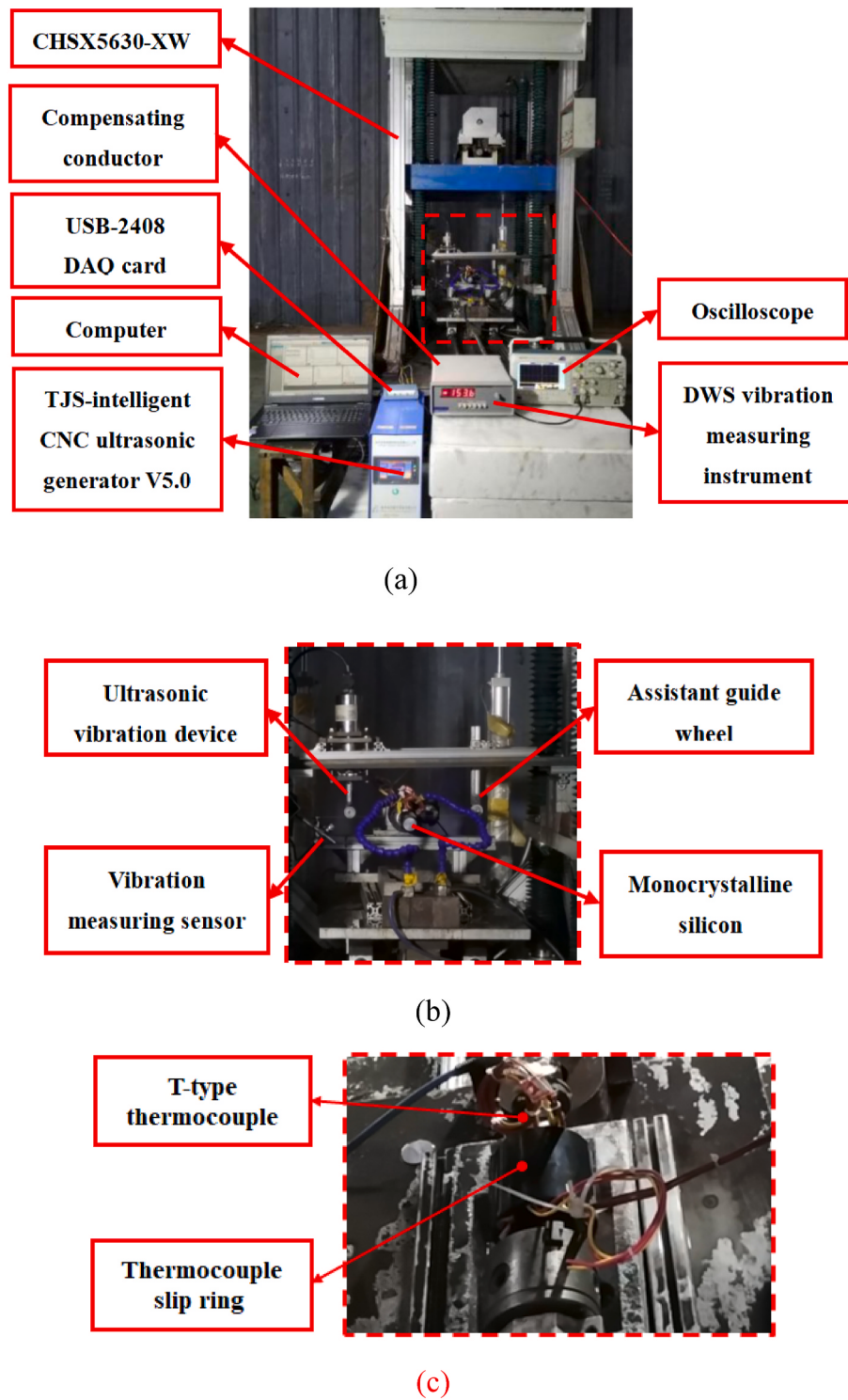


Fig. 9. Experiment devices.

**Table 2**  
Level of factors in experiment.

	vs(m/s)	vw(mm/min)	nw(r/min)
Level 1	2	1	10
Level 2	5	2	30
Level 3	8	3	50

boundary conditions and loading heat flux with the function of “birth-death element” in ANSYS software [19]. The results of temperature field obtained at each step are taken as the initial temperature field conditions for the next calculation step to simulate the continuous process of the wire sawing monocrystalline silicon.

### 2.3. The finite element model of monocrystalline silicon

Based on the mechanism of diamond wire sawing monocrystalline

**Table 3**  
Parameters & results of experiments.

Group number of experiments	$v_s$ (m/s)	$v_w$ (mm/min)	$n_w$ (r/min)	UAW	Temperature of Position A(°C)	Temperature of Position B(°C)	Temperature of Position C(°C)	Temperature of Position D(°C)
I-1	2	2	30	✗	16.8	19.8	22.3	24.3
I-2				✓	19.4	21.9	23.9	26.2
II-1	5	2	30	✗	19.8	22.6	24.1	26.2
II-2				✓	21.2	23.5	25.5	27.6
III-1	8	2	30	✗	21.1	23.3	24.9	27.6
III-2				✓	22.8	25.7	27.6	29.9
IV-1	5	1	30	✗	19.1	21.3	22.2	23.4
IV-2				✓	20.9	22.2	23.9	25.4
V-1	5	3	30	✗	21.8	22.6	25	26.4
V-2				✓	23.7	23.9	25.8	27.9
VI-1	5	2	10	✗	18.5	20.6	21.8	24
VI-2				✓	20.3	22.9	24.1	26.4
VII-1	5	2	50	✗	19.5	22.9	24.9	27.9
VII-2				✓	21.6	24.5	26.4	28.5

silicon, a finite element model is built in ANSYS. The geometric model of the monocrystalline silicon is 33 mm in diameter and 65 mm in length. The width of the kerf is 0.45 mm, and the thickness of the wafer is set as 1 mm. The finite element model of monocrystalline silicon is shown in Fig. 3. The material parameters of monocrystalline silicon are set according to Table 1 [11]. The element type used in the model is SOLID 70. Meshes in the kerf are refined to increase the accuracy of the simulation. Moreover, each node on the model has a degree of a single temperature freedom, which is used to establish a heat conduction model.

#### 2.4. Boundary conditions

In the process of wire sawing monocrystalline silicon, the temperature distribution of workpiece changes continuously with the sawing time, the heat conduction and the convection in the sawing process. During simulation process, parameters such as material characteristics, heat flux, convective heat transfer coefficient and room temperature need to be input, and some results such as the temperature distribution of workpiece will be output. Therefore, the temperature field analysis of wire sawing monocrystalline silicon is a typical transient temperature field analysis. The boundary conditions are as follow [20]:

- 1) The initial temperature of workpiece is equal to the ambient temperature.
- 2) Heat is transferred from the contact area between the wire saw and the workpiece.
- 3) The circulating heat occurs on all free surfaces of the workpiece and the heat transfer coefficient varies with the experimental conditions and the environment.

In this paper, it is considered that the initial temperature of the workpiece is consistent with the ambient temperature and remains constant. Therefore, the temperature function is a constant function, whose value is the ambient temperature 13 °C as shown in Eq. (1). The transient heat exchange equation is shown in Eq. (2).

$$T(x, y, z, \tau) = 13^\circ\text{C}, \tau = 0 \quad (1)$$

$$\frac{\partial t}{\partial \tau} = \frac{1}{C(t)\rho} \left[ \frac{\partial}{\partial x} \left( \lambda \frac{\partial t}{\partial x} \right) + \frac{\partial}{\partial y} \left( \lambda \frac{\partial t}{\partial y} \right) + \frac{\partial}{\partial z} \left( \lambda \frac{\partial t}{\partial z} \right) \right] + \frac{q_n}{C(t)\rho} \quad (2)$$

Where,  $\tau$  is time,  $t$  is the temperature,  $C$  is the specific heat capacity,  $\lambda$  is the thermal conductivity,  $q_n$  is an internal heat source which is equal to zero under this situation.

In the sawing process, one end of the workpiece is closely attached to the fixture, so no convective heat transfer coefficient is set on this surface. Other surfaces of the workpiece are in direct contact with air where air convective heat transfer coefficient is introduced. When the sawing process begins, the convective heat transfer load will be replaced by the

heat flux load in the sawing area because of the friction between the diamond wire saw and workpiece. As sawing continuing, the wire saw keeps sawing to form a new sawed surface in the kerf, which causes the original heat flux load area is changed continuously into the heat convection load area to simulate accurately.

#### 2.5. The heat flux model and loading process

In the process of wire sawing monocrystalline silicon, the heat is mainly generated in the contact area between the wire saw and the workpiece, where the abrasive particles rub violently against the workpiece and the mechanical energy consumed is converted into heat energy. It is believed in the research of Toda, Y [9,18,19,21–23]. et al. that the heat generated by the continuous friction between the wire saw and the workpiece pass through the frictional contact area to the workpiece and causes the change in temperature of workpiece. The heat flow in this process is expressed by heat flux, that is, the heat energy passing through per unit area per unit time. The calculation formula of heat flux is shown in Eq. (3).

$$q = \epsilon \frac{W}{S\tau} = \epsilon \frac{F_t V + P_U}{S} \quad (3)$$

Where,  $q$  is the heat flux,  $\epsilon$  is a proportionality coefficient usually 1/2 to 2/3 [11],  $W$  is the total energy input to the system. For CWS, it is mainly the mechanical energy input by machine tool, while for UAWS, it also includes the energy input by ultrasonic vibration.  $S$  is the contact area,  $\tau$  is time,  $P_U$  is the power supplied to the wire saw from the ultrasonic vibration device,  $F_t$  is the tangential sawing force,  $V$  is the sawing speed, that is the relative speed of wire saw to the workpiece at the sawing point. The calculation process of some parameters are as follows:

- 1) The tangential sawing force  $F_t$

The tangential sawing force of the diamond wire saw when sawing monocrystalline silicon can be obtained from Eq. (4) and Eq. (5) [24]. Eq. (4) is the tangential sawing force in CWS and Eq. (5) is the tangential sawing force in UAWS.

$$F_{t-T} = \frac{v_s' l_c P_{valid} \bullet \rho_{saw} D_{ws}}{v_s} \int_0^{\frac{\pi}{2}} F_{tg}(\theta_g) \bullet d\theta_g \quad (4)$$

$$F_{t-U} = \frac{v_s' l_c P_{valid} \bullet \rho_{saw} D_{ws}}{v_s} \int_0^{\frac{\pi}{2}} F_{tg-U}(\theta_g) \bullet d\theta_g \quad (5)$$

Where,  $v_s'$  is the element speed of wire saw,  $l_c$  is the contact length between the wire saw and the workpiece.  $P_{valid}$  is the effective sawing probability of abrasive particles, which equals to the proportion of the total number of abrasive particles on the wire saw surface that are

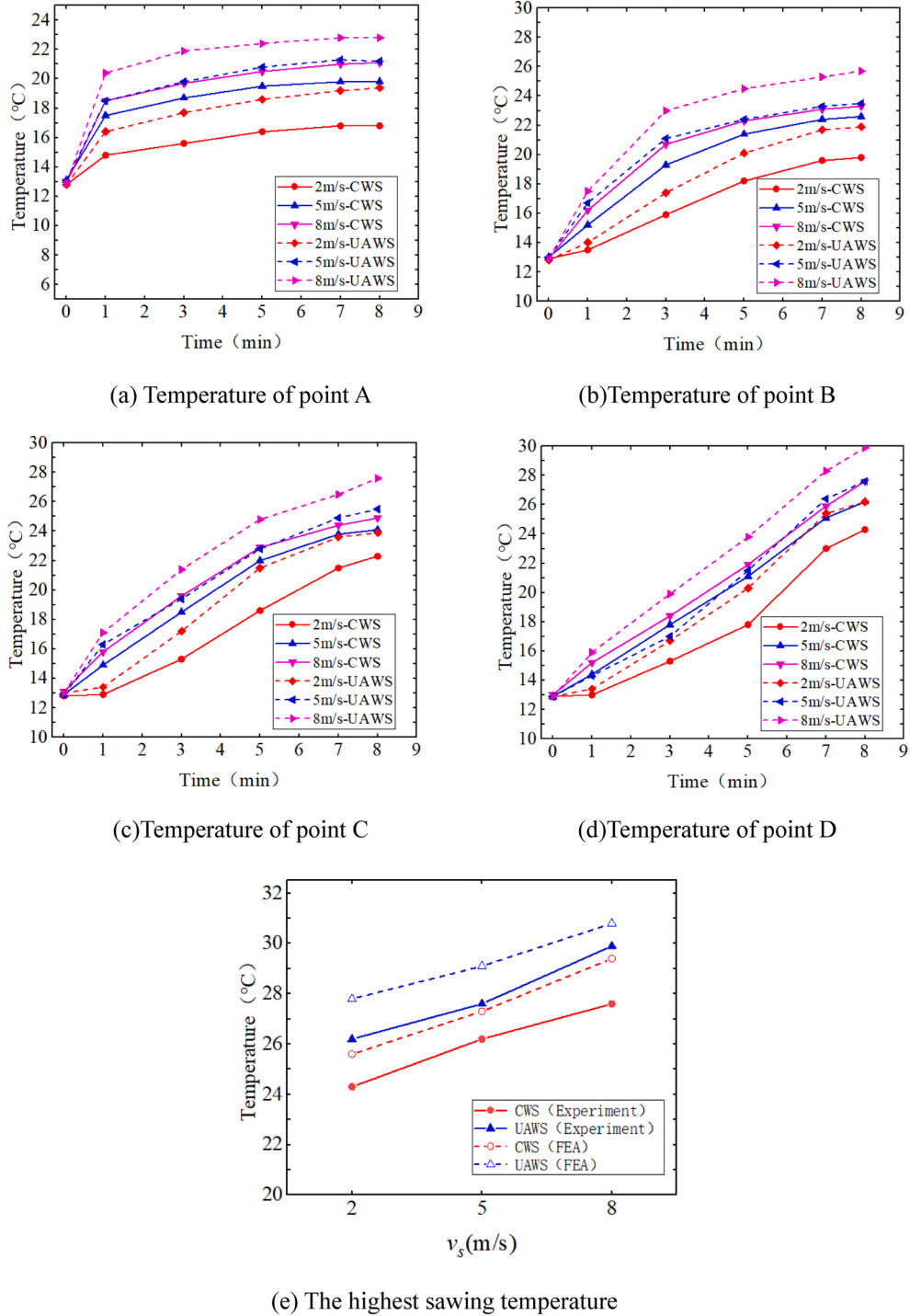


Fig. 10. Temperatures of different points under different  $v_s$ .

effectively engaged in sawing. It is generally believed that  $P_{valid}$  is between 0.1 and 0.5.  $\rho_{saw}$  is the distribution density of abrasive particles on the wire saw surface,  $D_{ws}$  is the average nominal diameter of wire saw,  $v_s$  is wire saw speed,  $F_{tg}$  is micro tangential grinding force of single abrasive particle.

## 2) The sawing speed $V$

When the wire saw the workpiece, the sawing speed of the wire saw is:

$$\begin{aligned} V &= v_s \pm \omega_w \bullet R_\tau \\ R_\tau &= R_0 - v_w \bullet \tau \end{aligned} \quad (6)$$

Where,  $v_s$  is wire saw speed,  $\omega_w$  is the angular velocity at which the workpiece is rotating, “-” represents that the linear velocity of the workpiece at the sawing point is in the same direction as the wire saw speed, while “+” is opposite.  $R_\tau$  is the radius of the saw point, that is, the length from the sawing point to the center of workpiece.  $R_0$  is the initial radius of the workpiece,  $v_s$  is feed rate,  $\tau$  is sawing time.

## 3) The contact area $S$

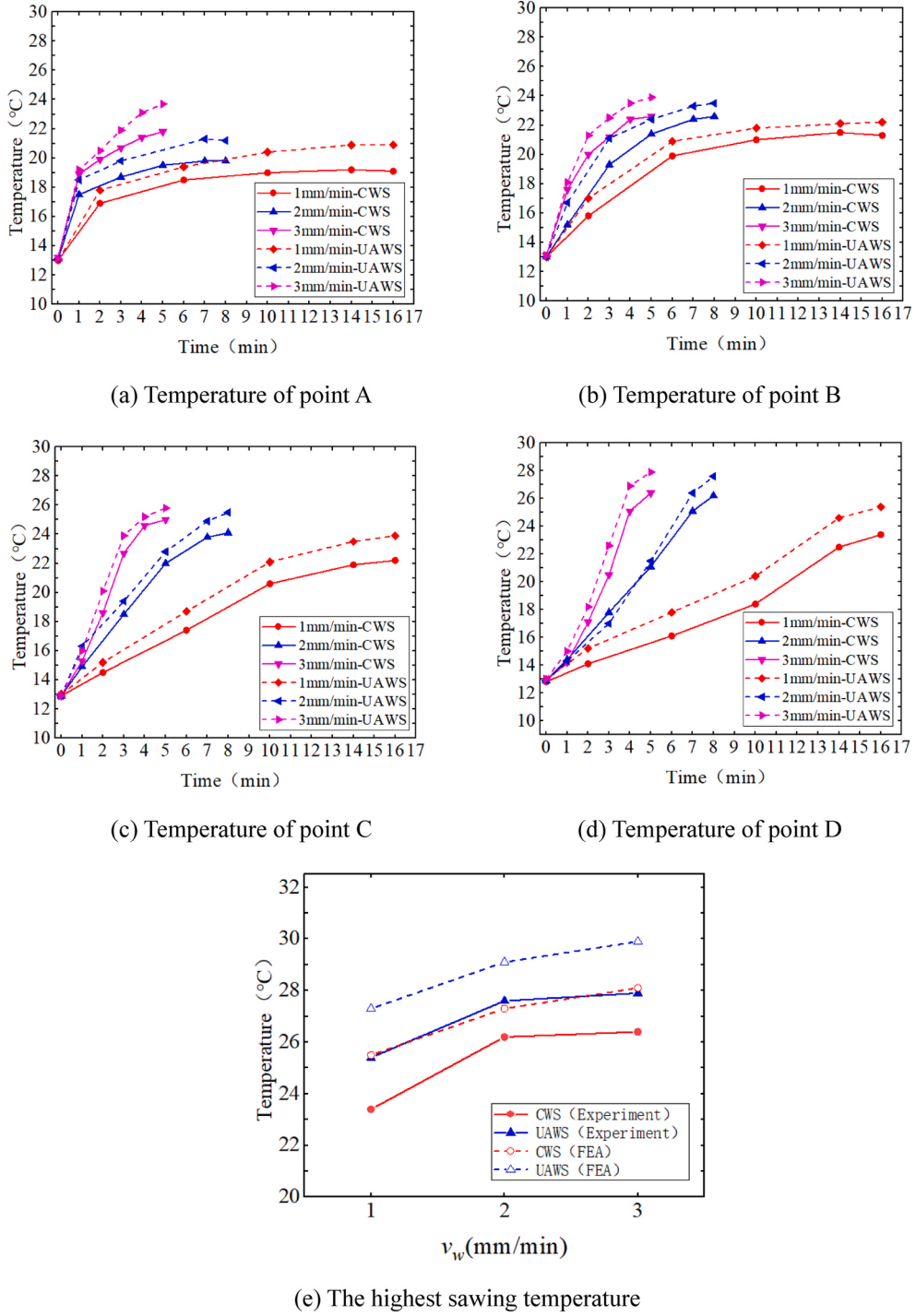


**Fig. 11.** Temperatures of different positions under different  $v_w$ .

Since the feed speed of the wire saw is relatively small, it can be considered that the sawing radius of the wire saw at the sawing point remains constant in a short time. The heat generated by sawing is transmitted to the workpiece through the contact area between the wire saw and the workpiece. The schematic of the contact area  $S$  is shown in Fig. 4. The contact area  $S$  between the wire saw and workpiece in a short period can be obtained from Eq. (7).

$$S = A \bullet l_c = \pi r \bullet \left( 2 \times \arcsin \frac{0.5F_n}{P} \bullet R_t + \omega_w \bullet \tau \bullet R_t \right) \quad (7)$$

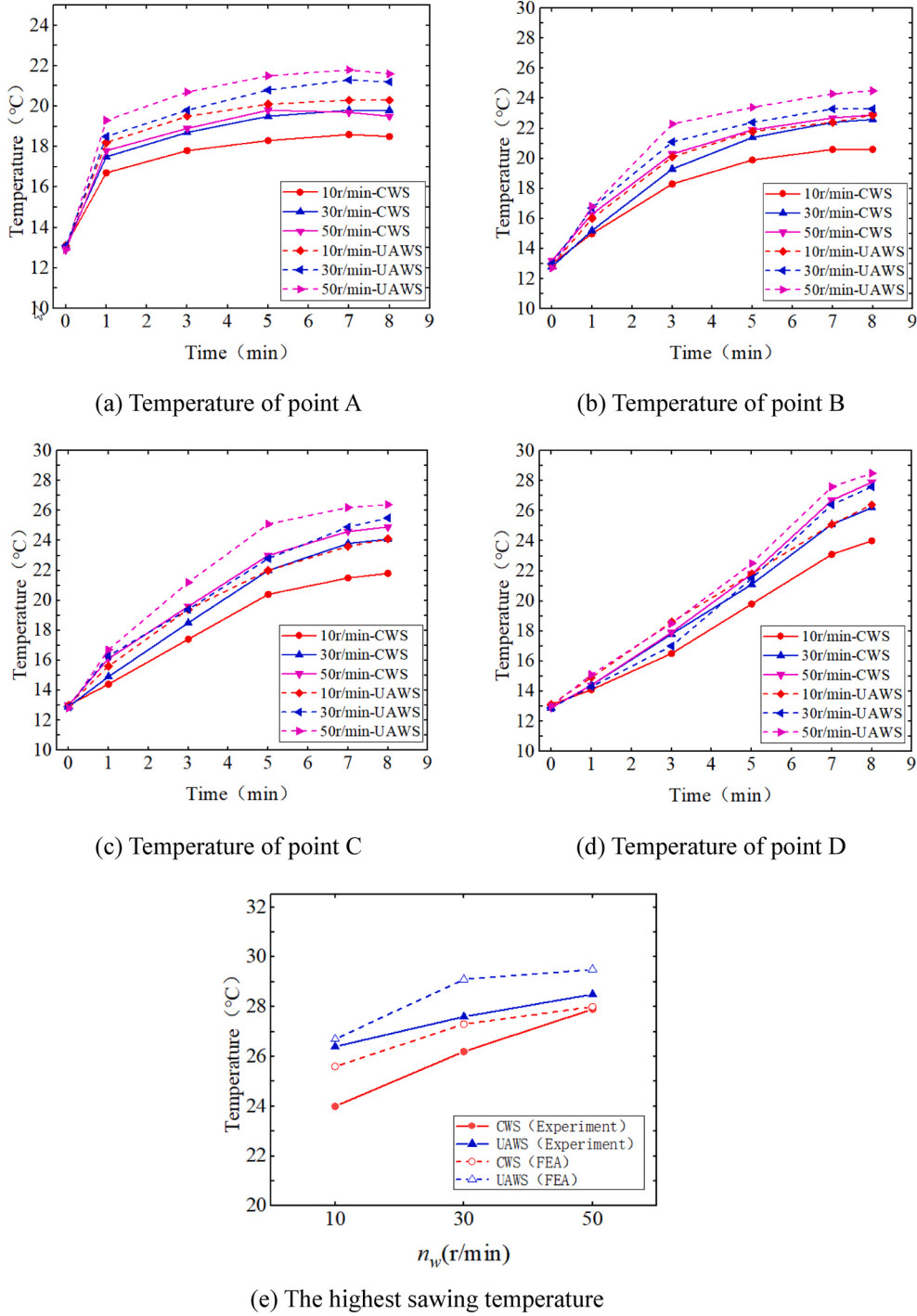
Where,  $A$  is the cross section curve of contact area,  $l_c$  is the contact

length,  $r$  is the radius of the wire saw,  $P$  is the tension force.

Substituting Eq. (4) ~ Eq. (7) into Eq. (3), The heat source model can be obtained.

$$q = \varepsilon \frac{F_t \bullet \left( v_s \pm \frac{30}{\pi} n_w R \right) + P_U}{\pi \bullet r \bullet \left( 2 \times \arcsin \frac{0.5F_n}{P} + \omega_w \bullet \tau \right) R} \quad (8)$$

#### 4) Loading process

Fig. 12. Temperatures of different positions under different  $n_w$ .

In order to simulate the process of wire sawing monocrystalline silicon, the “birth-death element” function of ANSYS was used to simulate the material removal in the kerf, and multiple load step is set for solution. “Birth-death element” means that elements are given the attribute of “birth” or “death”. The “death” element is not adopted in the solution process, that is, they will not play a role in the finite element calculation. The material removal process can be simulated more accurately by “birth-death element” function.

When establishing the geometric model of workpiece, the kerf was uniformly divided into 55 concentric layers along the radial direction, with 0.3 mm thickness of each layer. Those rings were integrated together by the GLUE operation in ANSYS. The elements of each layer

can be set as “birth” or “death” in every load step independently and the loading process is also independent on these elements. Simplifying model, it is assumed that the workpiece radius at the sawing point is always unchanged during the removal of one layer of workpiece, and the heat flux load is always applied to the torus outside the removed layer. During the sawing process, the part of workpiece that has been sawed and removed is set as a “death” element to simulate the state been removed. The elements that sawed off by wire saw keep being “killed” continuously to form a new workpiece surface. At the same time, the heat flux load is applied on the newly formed workpiece surface, while the original heat flux load area is changed into the heat convection load area, as shown in Fig. 5.

### 3. Experimental setup

In this paper, in order to measure the temperature in the kerf during sawing process, self-made thermocouples and corresponding instrument were used to measure the temperature and collect the data. As shown in Fig. 6, the monocrystalline silicon rob is sawed in half along the axis. Then, four grooves are located and sawed on the sawing surface of the half silicon rob and four T-type thermocouples with a diameter of 0.08 mm are fixed in the grooves respectively. The distance between the temperature measuring solder joint of T-type thermocouples and the end face of silicon rob is 1 mm, that is, the thickness of the wafer for each subsequent sawing experiment. The position of the four temperature measuring points A, B, C and D in the experiment is just the position of the solder joints of the thermocouples. Two half silicon robs were rejoined and clamped by the fixture then a group of experiments will be done. After these experiments were completed, those two half silicon robs were separated again and the positions of solder joints were adjusted by the fixture for the next sawing experiment. Fig. 7 is the image of the four temperature measuring points.

The verification experiment of temperature measuring in UAWS monocrystalline silicon was conducted on an improved reciprocating diamond wire saw machine tool CHSX5630-XW. Here are some technique index of the machine tool: The reciprocating speed of wire saw is 2–8 m/s. The feed rate of the workpiece is 1–3 mm/min. The rotation speed of the workpiece is 10–30 r/min. The wire saw is fixed diamond wire saw with a diameter of 0.47 mm. The workpiece is undoped cylindrical monocrystalline silicon with a diameter of 33 mm and a length of 65 mm. The ultrasonic vibration device includes the TJS-intelligent CNC ultrasonic generator V5.0, its supporting transducer and an ultrasonic horn, which are fixed and installed on the machine tool by trimmer bracket and profiles. During the experiment, the vibration state of the wire saw was monitored online by the DWS vibration measuring instrument and oscilloscope to ensure that the wire saw is always keeping ultrasonic vibration. As shown in Fig. 8, T-type thermocouples, T-type thermocouple slip ring, compensation wires, USB-2408 data acquisition card and software matching with the data acquisition card were used to collect and process the temperature data during the experiment. The machine tool and experiment devices are shown in Fig. 9.

Fig. 9(b) is a larger version of Fig. 9(a) and (c) is a larger version of Fig. 9(a) seen from back. Three important parameters were selected as variables: the wire saw speed  $v_s$  (m/s), the feed rate of the workpiece  $v_w$  (mm/min), and the rotation speed of the workpiece  $n_w$  (r/min). Three different values were selected for each process parameter, covering the range of common machining parameters and evenly distributed within the optional range, as shown in Table 2. In order to study the influence of a single process parameter on the variation trend of temperature and control the experiment variables, the single factor experiment method was used to carry out the experiment. Seven working conditions (I ~ VII) were arranged and the thickness of the workpiece sawed in each experiment was 1 mm. Moreover, CWS and UAWS experiments were carried out respectively in each working condition for comparison.

## 4. Results and discussions

The effects of the wire saw speed, the feed rate of the workpiece and the rotation speed of the workpiece on the sawing temperature during sawing process were studied. And the results of CWS and UAWS under the same working condition were compared. The experimental results are shown in Table 3. The temperature of each point in Table 3 is the temperature measured when one sawing experiment is finished.

### 4.1. Effects of $v_s$ on sawing temperature

The effects of wire saw speed on the sawing temperature can be obtained by the results of group I, group II and group III in Table 3. The experimental conditions are as follow: wire saw speed  $v_s = 2$  m/s (group

I), 5 m/s (group II), 8 m/s (group III), the feed rate of the workpiece  $v_w = 2$  mm/min, the rotation speed of the workpiece  $n_w = 30$ r/min. Fig. 10 (ād) shows the temperature of each point measured under different wire saw speed obtained from the experiment. The results of experimental and simulated highest sawing temperatures are shown in Fig. 10 (e).

Fig. 10 shows that within a certain range of experimental parameters, the temperature at each point at the same measuring time gradually increases with the wire saw speed, but the rising trend tends to be flat in the later period. This is because of the increase of the wire saw speed leads to the increase of friction between the wire saw and the workpiece in unit time, and the increase in friction generates a large amount of heat, which causes the temperature to rise. However, more and more of the heat generated by sawing is carried away by the wire saw as the wire saw speed increases, which slows down the trend of temperature rise. As the wire saw speed increases, the sawing temperature of each point at the same sawing time in CWS increases averagely by 3.6 °C and that in UAWS increases averagely by 3.7 °C. The highest temperature is 27.6 °C and 29.9 °C, respectively.

### 4.2. Effects of $v_w$ on sawing temperature

The effects of wire saw speed on the sawing temperature can be obtained by the results of group II, group IV and group V in Table 3. The experimental conditions are as follow: wire saw speed  $v_s = 5$  m/s, the feed rate of the workpiece  $v_w = 1$  mm/min (group IV), 2 mm/min (group II), 3 mm/min (group V), and the rotation speed of the workpiece  $n_w = 30$ r/min. Fig. 11 (ād) shows the temperature of each point measured under different the feed rate of the workpiece obtained from the experiment. The results of experimental and simulated highest sawing temperatures are shown in Fig. 11 (e).

Fig. 11 shows that in a certain range of experimental parameters, the sawing temperature increases gradually as the feed rate of the workpiece increases. The reason is that the contact pressure between the wire saw and the workpiece increases with the increase in the feed rate of the workpiece, and the sawing resistance increases, generating more heat. As the feed rate of the workpiece increases, the sawing temperature of each point at the same sawing time in CWS increases averagely by 1.6 °C and that in UAWS increases averagely by 1.5 °C. The highest temperature is 26.4 °C and 27.9 °C, respectively.

### 4.3. Effects of $n_w$ on sawing temperature

The effects of wire saw speed on the sawing temperature can be obtained by the results of group II, group VI and group VII in Table 3. The experimental conditions are as follow: wire saw speed  $v_s = 5$  m/s, the feed rate of the workpiece  $v_w = 2$  mm/min, and the rotation speed of the workpiece  $n_w = 10$  r/min (group VI), 30r/min (group II), 50 r/min (group VII). Fig. 12 (ād) shows the temperature of each point measured under different the feed rate of the workpiece obtained from the experiment. The results of experimental and simulated highest sawing temperatures are shown in Fig. 12 (e).

Fig. 12 shows that the sawing temperature at each point at the same measuring time gradually rises with the increase of the rotation speed of the workpiece, but the rising trend also tends to be flat in the later period. The mechanism is that as the rotation speed of the workpiece increases, the area of friction increases in unit time, resulting in the increase of heat and temperature. However, when the rotation speed of the workpiece reaches higher, the strengthening of convective heat transfer between the workpiece and air leads to partial heat loss, which slows down the rising trend of the sawing temperature. The outer part of the workpiece has a tendency of temperature drop due to the enhancement of heat dissipation but the change of convective heat transfer with air inside the workpiece caused by the change of the rotation speed of the workpiece is not obvious because the kerf is very narrow, the decline of temperature is not obvious. As the rotation speed of the workpiece increases, the sawing temperature of each point at the

same sawing time in CWS increases averagely by 2.0 °C and that in UAWS increases averagely by 1.5 °C. The highest temperature is 27.9 °C and 28.5 °C, respectively.

In addition, Figs. 10–12 show that the sawing temperature of each temperature measured point in UAWS is about 1.5 °C averagely higher than that in CWS. This is because the energy input to the sawing system increases after the ultrasonic vibration is applied from the perspective of energy. The sawing trajectory of the wire saw changes under the excitation of ultrasonic vibration and the scratch between the wire saw and the side of the kerf increases leading to more heat generated by friction. However, ultrasonic vibration can improve the chip removal condition, which reduces the friction force between the chip and the workpiece in the machining gap. The decrease of sawing force in UAWS will reduce the generation of sawing heat leading to the not obvious difference between the sawing temperature of UAWS and that of CWS under the same sawing parameters. Within the range of technological parameters of the experiment, the temperature of each position keeps rising with the sawing time, and the overall trend of temperature distribution is gradually rising from the outside of the workpiece to the inside. The highest sawing temperature is about 15 °C–17 °C higher than the ambient temperature. The average error between the experimental and the simulated results is 8.6% and the maximum error is 14%, which verifies the finite element model.

## 5. Conclusion

- (1) In this paper, the model of heat source in fixed diamond wire sawing monocrystalline silicon is established. The finite element model of diamond wire sawing monocrystalline silicon is built and the sawing temperature is simulated by ANSYS software. The average error between the experimental and the simulated results is 8.6% and the maximum error is 14%.
- (2) It is found from diamond wire saw sawing experiment that in the range of experimental conditions, the highest sawing temperature in CWS increases by about 15 °C compared to the ambient temperature, and that in UAWS increases by about 17 °C.
- (3) The sawing temperature increases with the increase of the wire saw speed, the feed rate of the workpiece and the rotation speed of the workpiece. The sawing temperature in CWS increases averagely by 3.6 °C, 1.6 °C and 2.0 °C respectively. Moreover, the sawing temperature in UAWS increases averagely by 3.7 °C, 1.5 °C and 1.5 °C respectively. The highest sawing temperature in CWS and UAWS is 27.9 °C and 29.9 °C, which indicates that ultrasonic vibration will not significantly change the sawing temperature.

## CRediT authorship contribution statement

**Yan Wang:** Conceptualization, Methodology, Supervision, Writing – review & editing. **Li-Xing Song:** Investigation, Formal analysis, Visualization, Writing – original draft. **Jian-Guo Liu:** Resources, Data curation. **Rui Wang:** Visualization, Software. **Bo-Cheng Zhao:** Software, Data curation.

## Declaration of competing interest

The authors declare that they have no known competing financial interests or personal relationships that could have appeared to influence the work reported in this paper.

## References

- [1] Hao Wu, Wire sawing technology: a state-of-the-art review [J], *Precis. Eng.* (12) (2016) 1–9, <https://doi.org/10.1016/j.precisioneng.2015.08.008>.
- [2] Arkadeep Kumar, N. Shreyes, Melkote. Diamond Wire Sawing of Solar Silicon Wafers: A Sustainable Manufacturing Alternative to Loose Abrasive Slurry Sawing [J], Elsevier B.V., 2018, pp. 549–566, <https://doi.org/10.1016/j.promfg.2018.02.156>.
- [3] Z.J. Pei, S. Kassir, Milind Bhagavat, et al., An experimental investigation into soft-pad grinding of wire-sawn silicon wafers [J], *Int. J. Mach. Tool Manufact.* (2) (2004) 299–306, <https://doi.org/10.1016/j.ijmachtools.2003.09.006>.
- [4] Ping Wang, Shaoping Xiao, Rui Jia, et al., 18.88%-efficient Multi-Crystalline Silicon Solar Cells by Combining Cu-Catalyzed Chemical Etching and Post-treatment process[J], Elsevier Ltd, 2018, pp. 153–158, <https://doi.org/10.1016/j.solener.2018.04.049>.
- [5] Chunhui Chung, Gow Dong Tsay, Meng-Hsiu Tsai, Distribution of diamond grains in fixed abrasive wire sawing process [J], *Int. J. Adv. Manuf. Technol.* (9) (2014) 1485–1494, <https://doi.org/10.1007/s00170-014-5782-y>.
- [6] Fang Cao, Kexun Chen, Jingjiao Zhang, et al., Next-generation multi-crystalline silicon solar cells: diamond-wire sawing, nano-texture and high efficiency[J], *Sol. Energy Mater. Sol. Cell.* (2015) 132–138, <https://doi.org/10.1016/j.solmat.2015.05.030>.
- [7] LI Shujuan, TANG Aofei, LI Yan, Li Jun. Influence of Diamond Wiresaw Excited by Transverse Ultrasonic Vibrationon Cutting Force and Critical Cutting Depth of Hard and Brittle Materials [J], *Journal of Mechanical Engineering*, 2016, (3): 187–196. <https://doi.org/10.3901/JME.2016.03.187>.
- [8] S. Li, B. Wan, R.G. Landers, Surface roughness optimization in processing SiC monocrystal wafers by wire saw machining with ultrasonic vibration [J], *Proc. IME B. Eng. Manufact.* (5) (2013) 725–739, <https://doi.org/10.1177/0954405413508116>.
- [9] Sumeet Bhagavat, Imin Kao, A finite element analysis of temperature variation in silicon wafers during wiresaw slicing[J], *Machine tools & manufacture* 48 (2008) 95–106, <https://doi.org/10.1016/j.ijmachtools.2007.07.009>.
- [10] Baozhu Li, Feng Fen, Study on the technology of cutting silicon carbide crystal wafer[J], *Equipment for Electronic Products Manufacturing* 38 (12) (2009) 36–38, 48.
- [11] X. Huang, H. Huang, H. Guo, Simulation and experimental research on the slicing temperature of the sapphire with diamond wire[J], *Int. J. Comput. Methods* 15 (3) (2018) 18, <https://doi.org/10.1142/S021987621843003X>.
- [12] Jian-chen Wang, Xiao-lei Deng, Tao Wang, Research on temperature distribution in silicon wafers slicing with wire saw[J], *Modular Machine Tool & Automatic Manufacturing Technique* (9) (2013) 32–34+38.
- [13] Yu Jiang, M.A. Chun-xiang, L.I. Tao, Fea simulation of the silicon wire saw temperature field[J], *Modular Machine Tool & Automatic Manufacturing Technique* (3) (2010) 11–15.
- [14] X.U. Zonghua, Y. Chunyan, P. Wei, et al., Finite element simulation of the silicon wiresaw temperature field [J], *Machine Design and Manufacturing Engineering* (2013).
- [15] H. Huang, X. Li, X. Xu, An experimental research on the force and energy during the sapphire sawing using reciprocating electropolated diamond wire saw [J], *J. Manuf. Sci. Eng.* 139 (12) (2017), <https://doi.org/10.1115/1.4038109>.
- [16] Yoshihori Abe, et al., Effects of thermal deformation of multi-wire saw's wire guides and ingot on slicing accuracy[J], *Engineering Materials* 389 (2009) 442–447. <https://doi.org/10.4028/www.scientific.net/KEM.389-390.442>.
- [17] Shinya Moriyama, et al., Study on the slicing of sapphire using a wire tool [J], *Adv. Mater. Res.* 806 (2015) 333–337. <https://doi.org/10.4028/www.scientific.net/AMR.1136.333>.
- [18] T. Yamada, M. Fukunaga, T. Ichikawa, et al., Prediction of warping in silicon wafer slicing with wire-saw machine [J], *Theor. Appl. Mech.* 51 (2002) 251–258.
- [19] T. Yamada, F. Kinai, K. Furuno, et al., Warpage analysis of silicon wafer in ingot slicing by wire-saw machine[C], in: Aip Conference. American Institute of Physics, 2004, <https://doi.org/10.1063/1.1766734>.
- [20] J.H. Choi, I. Lee, Finite element analysis of transient thermoelastic behaviors in disk brakes [J], *Wear* 257 (1/2) (2004) 47–58, <https://doi.org/10.1016/j.wear.2003.07.008>.
- [21] Lin Yang, Xiaoguang Xie, Transient thermal analysis for grinding fabrication of hard and brittle material[J], *Infrared Laser Eng.* 43 (S1) (2014) 169–176.
- [22] Jingxin Ren, Renke Kang, Technology of Difficult to Machine Material [M], Electrical engineering publisher, Beijing, 2011, pp. 310–320.
- [23] Yan Wang, Jianhua Xie, Wei Xiong, Lin Yang, Sheng Zhang, Research on simulation of heat source model based on finite element method in surface grinding [J], *J. Syst. Simul.* 28 (11) (2016) 2709–2715+2722.
- [24] Yan Wang, Li De-Lin, Zi-Jun Ding, Jian-Guo Liu, Rui Wang, Modeling and verifying of sawing force in ultrasonic vibration assisted diamond wire sawing (UAWS) based on impact load [J], *Int. J. Mech. Sci.* 164 (2019), <https://doi.org/10.1016/j.ijmecsci.2019.105161>.